Phenomenology of two-dimensional stably stratified turbulence under large-scale forcing

Kumar, A., Verma, M. K. & Sukhatme, J.

Original citation & hyperlink:
Kumar, A, Verma, MK & Sukhatme, J 2017, 'Phenomenology of two-dimensional stably stratified turbulence under large-scale forcing' Journal of Turbulence, vol. 18, no. 3, pp. 219-239.
https://dx.doi.org/10.1080/14685248.2016.1271123

DOI 10.1080/14685248.2016.1271123
ESSN 1468-5248

Publisher: Taylor and Francis

This is an Accepted Manuscript of an article published by Taylor & Francis in Journal of Turbulence on 10/01/2017, available online: http://www.tandfonline.com/10.1080/14685248.2016.1271123

Phenomenology of two-dimensional stably stratified turbulence under large-scale forcing

Abhishek Kumar[1,*], Mahendra K. Verma[1], and Jai Sukhatme[2,3]
[1]Department of Physics, Indian Institute of Technology, Kanpur 208016, India
[2]Centre for Atmospheric and Oceanic Sciences, Indian Institute of Science, Bangalore 560012, India.
[3]Divecha Centre for Climate Change, Indian Institute of Science, Bangalore 560012, India.

Abstract

In this paper we characterize the scaling of energy spectra, and the interscale transfer of energy and enstrophy, for strongly, moderately and weakly stably stratified two-dimensional (2D) turbulence, restricted in a vertical plane, under large-scale random forcing. In the strongly stratified case, a large-scale vertically sheared horizontal flow (VSHF) co-exists with small scale turbulence. The VSHF consists of internal gravity waves and the turbulent flow has a kinetic energy (KE) spectrum that follows an approximate k^{-3} scaling with zero KE flux and a robust positive enstrophy flux. The spectrum of the turbulent potential energy (PE) also approximately follows a k^{-3} power-law and its flux is directed to small scales. For moderate stratification, there is no VSHF and the KE of the turbulent flow exhibits Bolgiano-Obukhov scaling that transitions from a shallow $k^{-11/5}$ form at large scales, to a steeper approximate k^{-3} scaling at small scales. The entire range of scales shows a strong forward enstrophy flux, and interestingly, large (small) scales show an inverse (forward) KE flux. The PE flux in this regime is directed to small scales, and the PE spectrum is characterized by an approximate $k^{-1.64}$ scaling. Finally, for weak stratification, KE is transferred upscale and its spectrum closely follows a $k^{-2.5}$ scaling, while PE exhibits a forward transfer and its spectrum shows an approximate $k^{-1.6}$ power-law. For all stratification strengths, the total energy always flows from large to small scales and almost all the spectral indicies are well explained by accounting for the scale dependent nature of the corresponding flux.

*Email: abhishek.kir@gmail.com

1 Introduction

Stable stratification with rotation is an important feature of geophysical flows [1]. The strength of stratification is usually measured by the non-dimensional parameter called Froude number (Fr), which is defined as the ratio of the time scale of gravity waves and the nonlinear time scale. Strong stratification has $\mathrm{Fr} \ll 1$, while weak stratification has $\mathrm{Fr} \geq 1$ [2]. In this paper we restrict ourselves to two-dimensional (2D) stable stratification in a vertical plane [3, 4], this allows us to explore a wide range of Fr and characterise the interscale transfer of energy and enstrophy, and the energy spectra in strongly, moderately, and weakly stratified scenarios.

Apart from a reduction in dimensionality, the 2D stratified system differs from the more traditional three-dimensional (3D) equations in that it lacks a vortical mode. Indeed, the decomposition of the 3D system into vortical and wave modes [5, 6, 2] has proved useful in studying stratified [7, 8, 9, 10, 11] and rotating-stratified [12, 13, 14, 15, 16, 17] turbulence. The absence of a vortical mode implies that the 2D stratified system only supports nonlinear wave-wave mode interactions [18, 19] (interestingly, 3D analogs that only support wave interactions have also been considered previously [20, 21]). In a decaying setting, the initial value problem concerning the fate of a standing wave in 2D has been studied experimentally [22] and numerically [23, 24]. The regime was that of strong stratification, and not only where the waves observed to break, this process was accompanied by a forward energy transfer due to nonlocal parametric subharmonic instability [23]. Further, at long times after breaking, the turbulence generated was characterised by a $k_{\|}^{-3}$ scaling [24] (i.e., parallel to the direction of ambient stratification). Other decaying simulations, that focussed on the formation and distortion of fronts from an initially smooth profile, noted a self-similarity in the probability density function of the vorticity field as well as more of an isotropic $k^{-5/3}$ kinetic energy (KE) spectrum, though at early stages in the evolution of the system [25].

With respect to the forced problem, the case of random small scale forcing has been well studied. Specifically, at moderate stratification, the 2D system developed a robust vertically sheared horizontal flow (VSHF; [13]) accompanied by an inverse transfer of KE and a $k^{-5/3}$ scaling [26]. For weak stratification, a novel flux loop mechanism involving the upscale transfer of KE (with $k^{-5/3}$ scaling) and the downscale transfer of potential energy (PE), also with $k^{-5/3}$ scaling, was seen to result in a stationary state [27]. In fact, moisture driven strongly stratified flows in 2D have also been seen to exhibit an upscale KE transfer with a $k^{-5/3}$ scaling [28]. Interestingly, large-scale forcing in the form of a temperature gradient has been examined experimentally. Specifically, using a soap film, Zhang *et al.* [29] reported scaling of density fluctuations at low frequencies with exponents $-7/5$ (Bolgiano scaling [30, 31]) and -1 (Batchelor scaling [32]) for moderate and strong temperature gradients, respectively. Seychelles *et al.* [33] noted a similar scaling, and the development of isolated coherent vortices on a curved 2D soap bubble.

For quasi-two-dimensional (quasi-2D) stably stratified turbulence (i.e., flows

contained in a skewed aspect ratio box) Lindborg [34] performed simulations at the horizontal Froude numbers ranging approximately from 10^{-2} to 10^{-3}, i.e., in a very strongly stratified regime. It was observed that the horizontal kinetic and potential energy spectra followed $k_\perp^{-5/3}$ scaling (i.e., perpendicular to the ambient stratification), while the vertical kinetic and potential energy spectra followed $k_\parallel^{-3}$ scaling (see also [35, 36]). Further, in this quasi-2D setting, Vallgren *et al.* [16] added rotation to strong stratification in an attempt to explain the observed atmospheric kinetic and potential energy spectra.

In the present work, we look at the relatively unexamined case of random forcing at large scales for 2D stably stratified turbulence. The flows are simulated using a pseudospectral code Tarang [37] for strongly, moderately and weakly stratified scenarios. For strong stratification, a VSHF (identified as internal gravity waves) emerges at large scales and co-exists with small scale turbulence. The turbulent flow is characterized by a forward enstrophy cascade, zero KE flux and a KE spectrum that scales approximately as k^{-3}. The PE spectrum also follows an approximate k^{-3} power-law with a scale dependent flux of the form k^{-2}. At moderate stratification, there is no VSHF, and the KE spectrum shows a modified form of Bolgiano-Obukhov [30, 31] scaling for 2D flows—approximately $k^{-11/5}$ at large scales and k^{-3} at small scales in a similar manner as in 3D [38]. The KE flux also changes character with scale, and exhibits an inverse (forward) transfer at large (small) scales. The PE spectrum follows an approximate $k^{-1.64}$ scaling and its flux is weakly scale dependent. Finally, for weak stratification, the KE flux is upscale for most scales and its spectrum is characterized by a -2.5 exponent. The PE flux continues to be downscale and its spectrum obeys an approximate $k^{-1.6}$ scaling. All exponents observed are well explained by taking into account the variable nature of the corresponding flux. Exceptions are the PE spectra for moderate and weak stratification whose scaling is little steeper than expected.

The outline of the paper is as follows: In Sec. 2, we describe the equations governing stably-stratified flows and the associated parameters. In Sec. 3, we discuss the numerical details of our simulations. In the subsequent three subsections, we detail various kinds of flows observed for strongly stably-stratified flows in Sec. 4.1, moderately stably-stratified flows in Sec. 4.2, and weakly stably-stratified flows in Sec. 4.3. Finally, we conclude in Sec. 5 with a summary and discussion of our results.

2 Governing Equations

We employ the following set of equations to describe 2D stably stratified flows [39]:

$$\frac{\partial \mathbf{u}}{\partial t} + (\mathbf{u}\cdot\nabla)\mathbf{u} = -\frac{1}{\rho_0}\nabla p - \frac{\rho}{\rho_0} g\hat{z} + \nu\nabla^2\mathbf{u} + \mathbf{f}_u, \tag{1}$$

$$\frac{\partial \rho}{\partial t} + (\mathbf{u}\cdot\nabla)\rho = -\frac{d\bar{\rho}}{dz} u_z + \kappa\nabla^2\rho, \tag{2}$$

$$\nabla\cdot\mathbf{u} = 0, \tag{3}$$

where $\mathbf{u}$ is the 2D velocity field, p is the pressure, ρ and ρ_0 are the the fluctuating and background densities respectively, $\hat{z}$ is the buoyancy direction while $\hat{x}$ is the horizontal direction, $\mathbf{f}_u$ is the external force field, g is the acceleration due to gravity, and ν and κ are the kinematic viscosity and thermal diffusivity, respectively. In the above description, we make the Boussinesq approximation under which the density variation of the fluid is neglected except for the buoyancy term. Also, $d\bar{\rho}/dz < 0$ due to stable stratification.

The linearised version of the Eqs. (1-3) yield internal gravity waves for which the velocity and density fluctuate with the Brunt Väisälä frequency N defined using,

$$N^2 = -\frac{g}{\rho_0}\frac{d\bar{\rho}}{dz}. \tag{4}$$

The linearised equations also yield a dispersion relation for the internal gravity waves as,

$$\Omega = N\frac{k_x}{k}, \tag{5}$$

where $k = \sqrt{k_x^2 + k_z^2}$.

For simplification, we convert density to units of velocity by a transformation [40]:

$$b = \frac{g}{N}\frac{\rho}{\rho_0}. \tag{6}$$

Thus, in terms of b, the Eqs. (1) and (2) become

$$\frac{\partial \mathbf{u}}{\partial t} + (\mathbf{u}\cdot\nabla)\mathbf{u} = -\frac{1}{\rho_0}\nabla p - bN\hat{z} + \nu\nabla^2\mathbf{u} + \mathbf{f}_u, \tag{7}$$

$$\frac{\partial b}{\partial t} + (\mathbf{u}\cdot\nabla)b = Nu_z + \kappa\nabla^2 b. \tag{8}$$

In the limiting case of $\nu = \kappa = 0$ and $\mathbf{f}_u = 0$, only the total energy

$$E = \frac{1}{2}\int (u^2 + b^2) d\mathbf{r} \tag{9}$$

is conserved. This is in contrast to the 2D inviscid Navier Stokes equation that has two conserved quantities—the kinetic energy $\int d\mathbf{r}(u^2/2)$ and the enstrophy

$\int d\mathbf{r}(\nabla\times\mathbf{u})^2/2)$ [41]. Based on these two conservation laws, Kraichnan [41] deduced a dual energy spectrum for 2D hydrodynamic turbulence—$C_1\Pi_u^{2/3}k^{-5/3}$ for $k<k_f$, and $C_2\Pi_\omega^{2/3}k^{-3}$ for $k>k_f$. Here Π_u and Π_ω are the energy flux and enstrophy flux, respectively, k_f is the forcing wavenumber, and C_1 and C_2 are constants that have been estimated as 5.5–7.0 [42, 43] and 1.3–1.7 [44, 45], respectively.

The important nondimensional variables used for describing stably stratified flows are,

$$\text{Prandtl number Pr} = \frac{\nu}{\kappa}, \tag{10}$$

$$\text{Rayleigh number Ra} = \frac{N^2d^4}{\nu\kappa}, \tag{11}$$

$$\text{Reynolds number Re} = \frac{u_{rms}d}{\nu}, \tag{12}$$

$$\text{Froude number Fr} = \frac{u_{rms}}{Nd}, \tag{13}$$

$$\text{Richardson number Ri} = \frac{1}{\text{Fr}^2}, \tag{14}$$

$$\text{Buoyancy Reynolds number Re}_\text{b} = \text{ReFr}^2, \tag{15}$$

where u_{rms} is the rms velocity of flow, which is computed as a volume average. Note that the Rayleigh number is the ratio of the buoyancy and the viscous force, while the Richardson number is the ratio of the buoyancy and the nonlinearity $(\mathbf{u}\cdot\nabla)\mathbf{u}$.

It is convenient to work with nondimensional equations using box height d as a length scale, Nd as a velocity scale, and $-(d\bar{\rho}/dz)d$ as the density scale, which leads to $\mathbf{u}=\mathbf{u}'Nd$, $\rho=-\rho'(d\bar{\rho}/dz)d$, $\mathbf{x}=\mathbf{x}'d$, and $t=t'/N$. Hence the nondimensionalized version of Eqs. (1)-(3) are

$$\frac{\partial\mathbf{u}'}{\partial t'}+(\mathbf{u}'\cdot\nabla')\mathbf{u}' = -\nabla' p'-\rho'\hat{z}+\sqrt{\frac{\text{Pr}}{\text{Ra}}}\nabla'^2\mathbf{u}'+\mathbf{f}_u', \tag{16}$$

$$\frac{\partial\rho'}{\partial t'}+(\mathbf{u}'\cdot\nabla')\rho' = u_z'+\frac{1}{\sqrt{\text{RaPr}}}\nabla'^2\rho', \tag{17}$$

$$\nabla'\cdot\mathbf{u}' = 0. \tag{18}$$

In the above set of equations, the control parameters of the system are Ra, Pr, and ε, the energy supply rate by the external forcing $\mathbf{f}_u'$ (see Eq. (37) for details of forcing scheme). The Reynolds number Re and the Froude number Fr are the response parameters. We compute Re and Fr using following formula:

$$\text{Re} = \frac{u_{rms}d}{\nu}=u_{rms}'\frac{Nd^2}{\nu}=u_{rms}'\sqrt{\frac{\text{Ra}}{\text{Pr}}}, \tag{19}$$

$$\text{Fr} = \frac{u_{rms}}{Nd}=u_{rms}'. \tag{20}$$

Note that, in the dimensionless form the Froude number is the rms velocity

of the fluid. From this point onward we drop the primes on the variables for convenience.

In this paper we solve the above equations numerically, and study the energy spectra and fluxes in the regimes of strong stratification, moderate stratification, and weak stratification. Note that the KE spectrum $E_K(k)$, the horizontal KE spectrum $E_{K_h}(k)$, the vertical KE spectrum $E_{K_v}(k)$, and the potential energy (PE) spectrum $E_P(k)$ are defined as

$$E_K(k) = \sum_{k-1<k'\leq k} \frac{1}{2}|u(\mathbf{k}')|^2, \tag{21}$$

$$E_{K_h}(k) = \sum_{k-1<k'\leq k} \frac{1}{2}|u_x(\mathbf{k}')|^2, \tag{22}$$

$$E_{K_v}(k) = \sum_{k-1<k'\leq k} \frac{1}{2}|u_z(\mathbf{k}')|^2, \tag{23}$$

$$E_P(k) = \sum_{k-1<k'\leq k} \frac{1}{2}|\rho(\mathbf{k}')|^2. \tag{24}$$

In Fourier space, the equation for the kinetic energy $E_K(k)$ of the wavenumber shell of radius k is derived from Eq. (16) as [46, 47]

$$\frac{\partial E_K(k)}{\partial t} = T_K(k) + F_B(k) + F_{ext}(k) - D(k), \tag{25}$$

where $T_K(k)$ is the energy transfer rate to the shell k due to nonlinear interaction, and $F_B(k)$ and $F_{ext}(k)$ are the energy supply rates to the shell from the buoyancy and external forcing $\mathbf{f}_u$ respectively, i.e.,

$$F_B(k) = \sum_{|\mathbf{k}|=k} \Re(\langle u_z(\mathbf{k})\rho^*(\mathbf{k})\rangle), \tag{26}$$

$$F_{ext}(k) = \sum_{|\mathbf{k}|=k} \Re(\langle \mathbf{u}(\mathbf{k})\cdot \mathbf{f}_u{}^*(\mathbf{k})\rangle). \tag{27}$$

In Eq. (25), $D(k)$ is the viscous dissipation rate defined by

$$D(k) = \sum_{|\mathbf{k}|=k} 2\nu k^2 E_K(k). \tag{28}$$

The kinetic energy flux $\Pi_K(k_0)$, which is defined as the kinetic energy leaving a wavenumber sphere of radius k_0 due to nonlinear interaction, is related to the nonlinear interaction term $T_K(k)$ as

$$\Pi_K(k) = -\int_0^k T_K(k)dk. \tag{29}$$

Under a steady state $[\partial E_K(k)/\partial t = 0]$, using Eqs. (25) and (29), we deduce that

$$\frac{d}{dk}\Pi_K(k) = F_B(k) + F_{ext}(k) - D(k) \tag{30}$$

or

$$\Pi_K(k+\Delta k) = \Pi_K(k) + (F_B(k) + F_{ext}(k) - D(k))\Delta k. \tag{31}$$

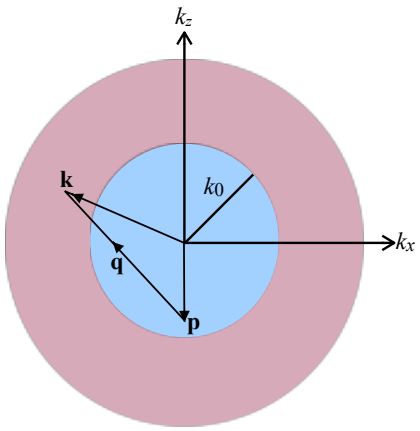

Figure 1: Schematic diagram of the energy flux from a wavenumber sphere of radius k_0. The blue region denotes the modes inside the sphere, and the red region the modes outside the sphere.

In computer simulations, the KE flux, $\Pi_K(k_0)$, is computed by the following formula, using *mode-to-mode* energy transfer procedure [48, 49],

$$\Pi_K(k_0) = \sum_{k>k_0} \sum_{p\le k_0} \delta_{\mathbf{k},\mathbf{p}+\mathbf{q}} \Im([\mathbf{k}\cdot\mathbf{u}(\mathbf{q})][\mathbf{u}^*(\mathbf{k})\cdot\mathbf{u}(\mathbf{p})]). \tag{32}$$

Dar *et al.* [48] presented a very efficient technique to compute the above flux using a pseudospectral method. Specifically, Eq. (32) is written in terms of *truncated* variables $\mathbf{u}^>$ and $\mathbf{u}^<$, and reads,

$$\Pi_K(k_0) = \Im\left[\sum_{k>k_0} k_j \left\{u_i^>(\mathbf{k})\right\}^* \sum_{p\le k_0} u_j(\mathbf{k}-\mathbf{p}) u_i^<(\mathbf{p})\right]. \tag{33}$$

Here,

$$\mathbf{u}^>(\mathbf{k}) = \begin{cases} 0 & \text{if } k \le k_0, \\ \mathbf{u}(\mathbf{k}) & \text{if } k > k_0, \end{cases}$$

and,

$$\mathbf{u}^<(\mathbf{p}) = \begin{cases} \mathbf{u}(\mathbf{p}) & \text{if } p \le k_0, \\ 0 & \text{if } p > k_0. \end{cases}$$

The second summation of Eq. (33) (over p) is the convolution sum, which is computed using the Fast Fourier Transform [48, 49]. For clarity, Fig. 1 illustrates the triad interaction involved in an energy flux computations.

Similarly, the enstrophy flux $\Pi_\omega(k_0)$ and PE flux $\Pi_P(k_0)$ are the enstrophy and the potential energy leaving a wavenumber sphere of radius k_0, respectively. The formulae to compute these quantities are,

$$\Pi_\omega(k_0) = \sum_{k>k_0}\sum_{p\leq k_0}\delta_{\mathbf{k},\mathbf{p}+\mathbf{q}}\Im([\mathbf{k}\cdot\mathbf{u}(\mathbf{q})][\omega^*(\mathbf{k})\omega(\mathbf{p})]), \tag{34}$$

$$\Pi_P(k_0) = \sum_{k>k_0}\sum_{p\leq k_0}\delta_{\mathbf{k},\mathbf{p}+\mathbf{q}}\Im([\mathbf{k}\cdot\mathbf{u}(\mathbf{q})][\rho^*(\mathbf{k})\rho(\mathbf{p})]). \tag{35}$$

Note that the total energy flux $\Pi_{\text{Total}}(k)$ is defined as

$$\Pi_{\text{Total}}(k) = \Pi_K(k) + \Pi_P(k). \tag{36}$$

In the above expression, the prefactors are unity due to nondimensionalization. In the following sections, we compute the aforementioned spectra and fluxes using the steady-state numerical data.

3 Simulation Method

We solve Eqs. (16)-(18) numerically using a pseudo-spectral code Tarang [37]. In brief, the code employs a fourth-order Runge-Kutta method for time stepping, the Courant-Friedrichs-Lewy (CFL) condition to determine the time step Δt, and 2/3 rule for dealiasing. Finally, we use periodic boundary conditions on both sides of a square box of dimension $2\pi \times 2\pi$.

Since the system is stable, we apply random large-scale forcing in the band $2 \leq k \leq 4$ to obtain a statistically-steady turbulent flow using the following scheme,

$$\mathbf{f}_u(\mathbf{k}) = Ae^{i\Phi}\begin{pmatrix}\cos\vartheta\\ -\sin\vartheta\end{pmatrix}, \tag{37}$$

where ϑ is the angle between $\widehat{\mathbf{z}}$ and $\mathbf{k}$, Φ is the random phase in $[0, 2\pi]$ with zero mean, and,

$$A = \sqrt{\frac{2\varepsilon}{n_f \Delta t}}. \tag{38}$$

Here ε is the total energy supply rate and n_f is the total number of modes inside the forcing wavenumber band.

In Table 1 and Table 2 we list the set of parameters for which we performed our simulations. We employ grid resolutions of 512^2 to 8192^2, the higher ones for higher Reynolds number. The Rayleigh number of our simulations ranges from 10^8 to 10^{10}, while the Reynolds number ranges from 5000 to 3.7×10^4. All our simulations are fully resolved since $k_{max}\eta > 1$, where η is the Kolmogorov length scale, and k_{max} is the maximum wavenumber attained in DNS for a particular grid resolution. Note that the energy supply rate, ε, is greater than the viscous

Table 1: Parameters of our direct numerical simulations (DNS): Froude number Fr; grid resolution; Rayleigh number Ra; energy supply rate ε; Richardson number Ri; Reynolds number Re; buoyancy Reynolds number $\mathrm{Re_b}$; anisotropy ratio $A = \langle u_\perp^2 \rangle / \langle u_\parallel^2 \rangle$; and $k_{max}\eta$, where k_{max} is the maximum wavenumber and η is the Kolmogorov length. We kept the Prandtl number Pr = 1 for all our runs.

Fr	Grid	Ra	ε	Ri	Re	$\mathrm{Re_b}$	A	$k_{max}\eta$
0.16	512^2	10^9	10^{-6}	40	5.0×10^3	1.3×10^2	38	2.8
0.31	512^2	10^8	10^{-4}	11	3.1×10^3	3.0×10^2	38	3.7
0.37	8192^2	10^{10}	0.01	7.3	3.7×10^4	5.1×10^3	3.4	4.9
0.45	512^2	10^8	0.01	4.9	4.5×10^3	9.1×10^2	4.2	1.4
0.73	2048^2	10^8	0.1	1.9	7.3×10^3	4.0×10^3	1.6	3.8
1.1	2048^2	10^8	0.3	0.8	1.1×10^4	1.3×10^4	1.4	3.3

Table 2: Values of the kinetic energy E_K, the potential energy E_P, E_P/E_K, the kinetic energy dissipation rate ϵ_K, the potential energy dissipation rate ϵ_P, and ϵ_P/ϵ_K at different Froude number for all runs.

Fr	E_K	E_P	E_P/E_K	ϵ_K	ϵ_P	ϵ_P/ϵ_K
0.16	1.3×10^{-2}	8.8×10^{-4}	0.1	2.2×10^{-6}	1.7×10^{-7}	0.1
0.31	4.7×10^{-2}	4.5×10^{-3}	1.0	2.2×10^{-5}	6.2×10^{-6}	0.3
0.37	6.8×10^{-2}	3.8×10^{-2}	0.6	4.9×10^{-4}	2.8×10^{-3}	5.7
0.45	1.0×10^{-1}	3.8×10^{-2}	0.4	1.2×10^{-3}	2.9×10^{-3}	2.4
0.73	3.0×10^{-1}	2.0×10^{-1}	0.7	5.3×10^{-3}	2.7×10^{-2}	5.1
1.1	6.0×10^{-1}	4.0×10^{-1}	0.6	9.2×10^{-3}	7.7×10^{-2}	8.4

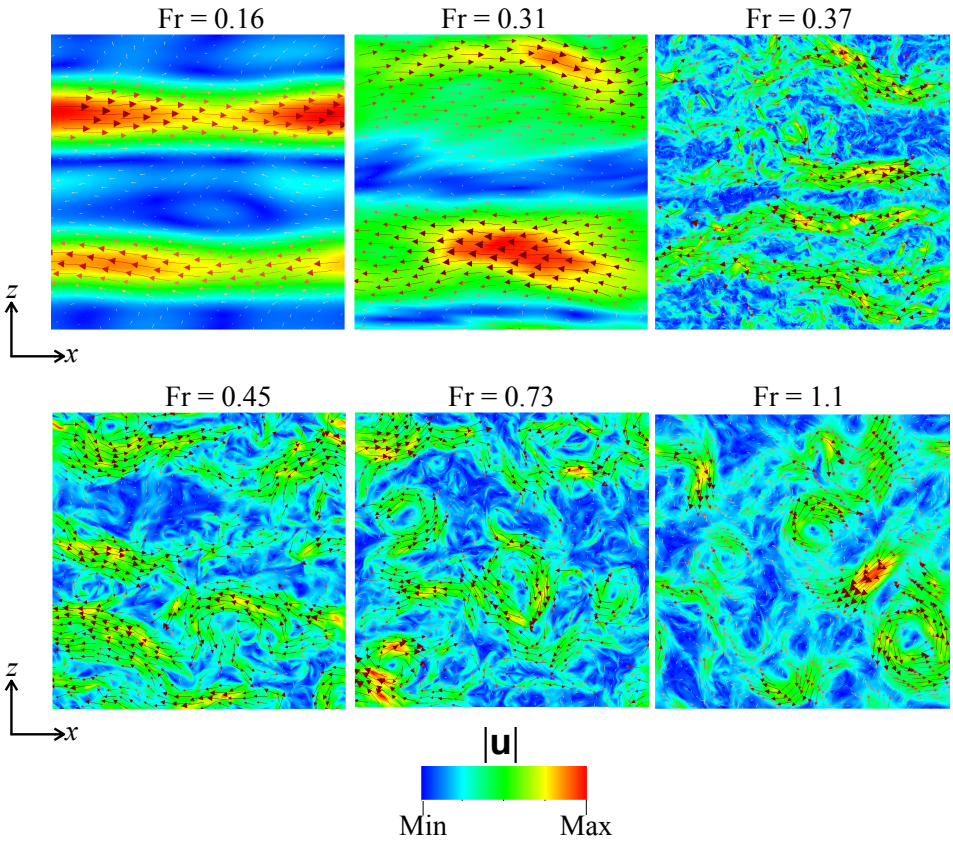

Figure 2: For Fr = 0.16, 0.31, 0.37, 0.45, 0.73, and 1.1, the density plots of the magnitude of velocity field with the velocity vector **u** superposed on it in the x-z plane. For low Fr, fluctuations are suppressed along buoyancy direction. However they grow gradually on the increase of Fr. We classify Fr = 0.16, 0.31 as strong stratification, 0.37 and 0.45 as moderate stratification, 1.1 as weak stratification, and 0.73 as transition between moderate and weak stratification.

dissipation rate, ϵ_u, with the balance getting transferred to the potential energy via buoyancy ($\rho g u_z/\rho_0$).

The Froude number of our simulations are Fr = 0.16, 0.31, 0.37, 0.45, 0.73, and 1.1; the lowest Fr correspond to the strongest stratification, while the largest Fr to the weakest stratification. We show in subsequent discussion that the flow behaviour in these regimes are very different. One of the major difference is the anisotropy that is quantified using an anisotropy parameter $A = \langle u_\perp^2 \rangle / \langle u_\parallel^2 \rangle$. For the strongest stratification with Fr = 0.16, $A \approx 38$ indicating a strong anisotropy. However, for the weakest stratification with Fr = 1.1, $A \approx 1.4$, indicating a near isotropy.

4 Results

We begin with a qualitative description of the flow profiles for the strongly, moderately, and weakly stratified regimes. In Fig. 2 we show the velocity vectors superposed on the magnitude of the velocity field. For strong stratification (Fr = 0.16), we observe two robust flow structures moving in the opposite directions, i.e., a VSHF [13]. On further increasing Fr to 0.31, the streams widen and start to diffuse. In the moderately stratified regime (Fr = 0.37, 0.45), the streams break into filaments, and the flow becomes progressively disordered. Finally, for weak stratification (Fr = 1.1), the flow appears turbulent during which the aforementioned filaments tend to be wrapped into compact isolated vortices [50]. The transition from moderate to weak stratification occur near Fr = 0.73.

4.1 Strong Stratification

Here we focus on the simulation with Fr = 0.16, Re = 5000, Pr = 1, Ra = 10^9, and forcing amplitude $\varepsilon = 10^{-6}$. The flow exhibits strong anisotropy as is evident from the ratio $A = \langle u_\perp^2 \rangle / \langle u_\parallel^2 \rangle = 38$. In fact, the flow exhibits wave-like behaviour that can be confirmed by studying the dominant Fourier modes.

We compute the most energetic Fourier modes in the flow and find the modes $(1, 0)$ and $(1, 1)$ to be the most dominant. Fig. 3 shows the time series of the real and imaginary parts of $\hat{u}_z(1, 1)$ and $\hat{u}_z(1, 0)$ from which we extract the oscillation time period of these modes as approximately 8.4 and 6.5, and their frequencies as 0.75 and 0.97. These numbers match very well with the dispersion relation [Eq. (5)], thus we interpret these structures to be internal gravity waves. Note that these robust flow structures moving in horizontal directions constitute the VSHF. We also observe that $\hat{\mathbf{u}}(0, n) \approx 0$ where n is an integer, so almost no energy is transferred to purely zonal flows. A natural vertical length-scale that emerges in strongly stratified flows is U/f, where U is the magnitude of the horizontal flow and $f = N/2\pi$ [51]. With the present parameters, we see that this leads to VSHFs of size ~ 1, which is in reasonable agreement with the bands seen in the first panel of Fig. 2.

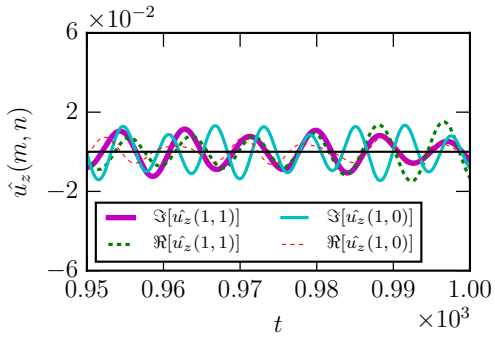

Figure 3: Time series of the real and imaginary parts of Fourier modes $\hat{u}_z(1,1)$ and $\hat{u}_z(1,0)$ for strong stratification (Fr $= 0.16$).

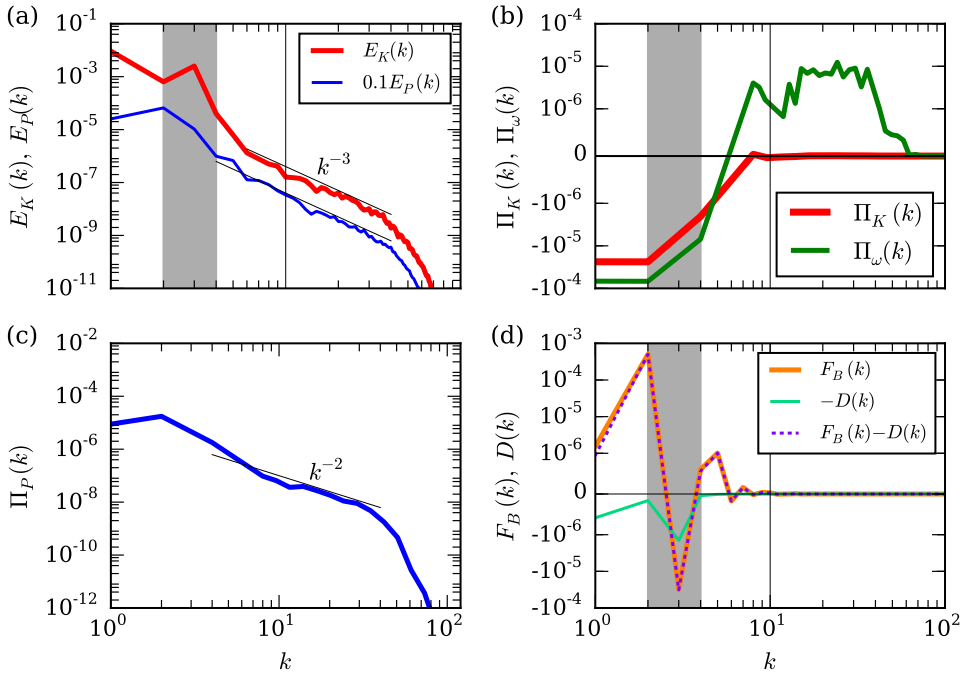

Figure 4: Strong stratification (Fr $= 0.16$): (a) KE and PE spectra; (b) KE flux $\Pi_K(k)$ and enstrophy flux $\Pi_\omega(k)$. The grey shaded region shows the forcing band. The KE flux is zero for wavenumber $k \geq 10$; (c) PE flux $\Pi_P(k)$; (d) $F_B(k)$, $D(k)$, and $F_B(k) - D(k)$.

To explore the flow properties further, we compute the KE spectrum $E_K(k)$, and the KE and enstrophy fluxes. As shown in Fig. 4(a), the KE at small scales (large k) is several orders of magnitude lower than that for low-k modes. Thus, even though small-scale turbulence is present in the system, the energy content of the large scale internal gravity waves is much larger than the sea of small-scale turbulence. The flux computations show that the KE flux $\Pi_K(k) \approx 0$ for $k > k_f$, but the enstrophy flux $\Pi_\omega(k)$ is positive and fairly constant [see Fig. 4(b)]. For these band of wavenumbers we observe that

$$E_K(k) \approx 1.0\Pi_\omega^{2/3}k^{-3}, \tag{39}$$

which is similar to the forward enstrophy cascade regime of 2D turbulence (including the prefactor) [44, 45]. The aforementioned flux computations are also consistent with the fluxes reported for 2D turbulence [52, 53, 54].

In addition, we observe that the PE spectrum, $E_P(k)$, scales approximately as k^{-3} and the PE flux follows $\Pi_P(k) \sim k^{-2}$ [see Fig. 4(a,c)]. The k^{-3} scaling of the PE is in sharp contrast to the k^{-1} Batchelor spectrum for a passive scalar in 2D hydrodynamic turbulence in the wavenumber regimes with a forward enstrophy cascade [32, 55]. Further, $\Pi_P(k)$ decreases rapidly with wavenumber, rather than being a constant as for a passive scalar. We demonstrate the consistency among these scalings of KE and PE as follows: the KE spectrum $E_K(k) \sim k^{-3}$ implies $u_k \sim k^{-1}$, substitution of which in the PE flux equation yields

$$\Pi_P \approx k u_k \rho_k^2 \sim k^{-2}. \tag{40}$$

Consequently, $\rho_k \sim k^{-1}$, and hence

$$E_P(k) \approx \frac{\rho_k^2}{k} \sim k^{-3}. \tag{41}$$

Also, Fig. 4(d) shows the energy supply rate due to buoyancy $F_B(k)$ and the dissipation rate $D(k)$. The buoyancy is active at large-scales only, and it is quite small for $k \geq 10$.

Given the anisotropic nature of the flow, we also compute the KE spectrum of the horizontal flow $E_{K_h}(k)$ and of the vertical flow $E_{K_v}(k)$, which are shown in Fig. 5. As expected, $E_{K_h}(k) > E_{K_v}(k)$. Further, $E_{K_h}(k) \sim k^{-3}$ and $E_{K_v}(k) \sim k^{-5}$. Indeed, the different spectral exponents of horizontal and vertical KE spectra show that the flow is anisotropic at all length scales.

So, for strong stratification, the picture that emerges is of large-scale internal gravity waves, physically manifested as a VSHF, that co-exist with small scale turbulence which is characterized by an approximate k^{-3} scaling for both the KE and PE. Moreover, the KE flux is close to zero while the PE flux is positive and closely follows a k^{-2} power-law. Thus, the total energy of the system is systematically transferred to small scales. Note that stably stratified turbulence in a channel also shows the coexistence of active turbulence and internal gravity waves [56]. The energetic dominance of the VSHF suggests strong anisotropy in the system and this is confirmed by the different scaling exponents of the

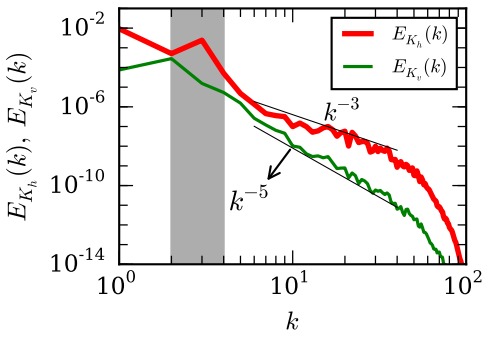

Figure 5: Plots for horizontal and vertical kinetic energy spectra for strong stratification (Fr = 0.16).

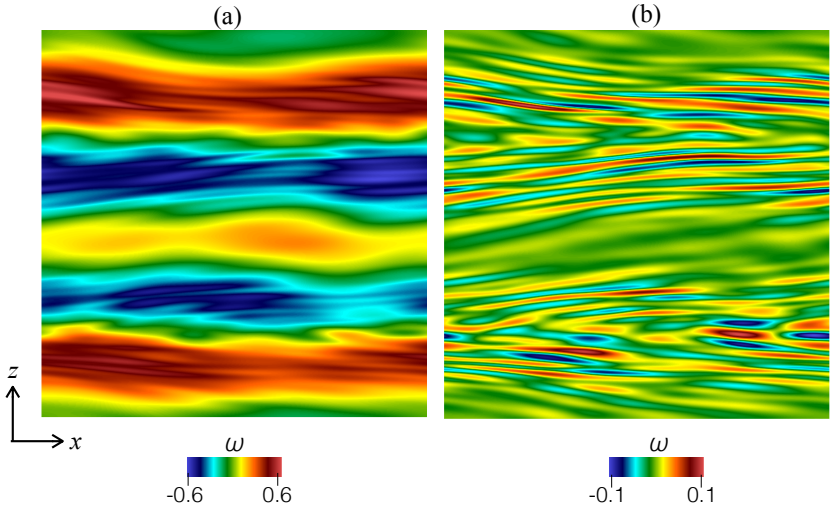

Figure 6: For Fr = 0.16, (a) density plot of the magnitude of vorticity field ω; (b) The density plot of the vorticity field ω; for this we truncate the modes in the wavenumber band $0 \leq k \leq 10$.

horizontal and vertical KE spectra. To visualize the coexistence of the large-scale internal gravity waves and small scale turbulence we plot the vorticity field in Fig. 6(a), and the small-scale vorticity field after removing the large-scale wavenumbers from the band $0 \leq k \leq 10$ in Fig. 6(b). Clearly we observe large-scale internal gravity waves or VSHF riding on a sea of small-scale turbulence.

4.2 Moderate Stratification

Among our simulations, the density stratification is moderate for Fr = 0.37 and 0.45 (see Fig. 2). In this subsection we will focus on Fr = 0.37 which is obtained for Ra = 10^{10} and an energy supply rate of $\varepsilon = 0.01$. For this case, Re = 3.7×10^4. As shown in Fig. 2, the flow pattern for the above set of parameters differs significantly from that corresponding to strong stratification. In fact, there is no evidence of a VSHF in Fig. 2 for Fr = 0.37.

With regard to turbulence phenomenology, Bolgiano [30] and Obukhov [31] (denoted by BO) were among the first to consider stably stratified flows in 3D. According to this phenomenology, for large scales, i.e., $k < k_B$,

$$E_K(k) = c_1 \left(\frac{g}{\rho_0}\right)^{4/5} \epsilon_P^{2/5} k^{-11/5}, \tag{42}$$

$$E_P(k) = c_2 \left(\frac{g}{\rho_0}\right)^{-2/5} \epsilon_P^{4/5} k^{-7/5}, \tag{43}$$

$$\Pi_K(k) = c_3 \left(\frac{g}{\rho_0}\right)^{6/5} \epsilon_P^{3/5} k^{-4/5}, \tag{44}$$

$$\Pi_P(k) = \epsilon_P = \text{constant}, \tag{45}$$

$$k_B = c_4 \left(\frac{g}{\rho_0}\right)^{3/2} \epsilon_K^{-5/4} \epsilon_P^{3/4}, \tag{46}$$

where c_i's are constants, ϵ_K is the kinetic energy supply rate, ϵ_P is the potential energy supply rate, and k_B is the Bolgiano wavenumber. At smaller scales ($k > k_B$), BO argued that the buoyancy effects are weak, and hence Kolmogorov's spectrum is valid in this regime, i.e.,

$$E_K(k) = C_u \epsilon_K^{2/3} k^{-5/3}, \tag{47}$$

$$E_P(k) = C_\rho \epsilon_K^{-1/3} \epsilon_P k^{-5/3}, \tag{48}$$

$$\Pi_K(k) = \epsilon_K = \text{constant}, \tag{49}$$

$$\Pi_P(k) = \epsilon_P = \text{constant}, \tag{50}$$

where C_u and C_ρ are Kolmogorov's and Batchelor's constants respectively. Note that the Bolgiano-Obukhov [30, 31] scaling is valid for nearly isotropic stably stratified turbulence. The recent developments [38, 57, 58, 59, 60] in 3D stably stratified turbulence, at moderate stratification, have confirmed the existence of BO scaling. For strongly stratified turbulence, Lindborg [34] shown that the horizontal KE and PE spectra exhibit $-5/3$ spectral exponent, while the vertical

KE and PE spectra exhibit -3 spectral exponent. Later, the direct numerical simulations of Brethouwer *et al.* [35] and Bartello and Tobias [36] also confirmed the Lindborg [34] scaling laws for strongly stratified turbulence.

For 2D stably stratified turbulence, Eqs. (47-50) need to be modified for the $k > k_B$ regime since 2D hydrodynamic turbulence yields k^{-3} energy spectrum at small scales due to constant enstrophy cascade. Thus, modifications of Eqs. (47-50) take the form,

$$E_K(k) = c_5 \Pi_\omega^{2/3} k^{-3}, \tag{51}$$
$$E_P(k) = c_6 k^{-1}, \tag{52}$$
$$\Pi_\omega(k) = \epsilon_\omega = \text{constant}, \tag{53}$$
$$\Pi_P(k) = \epsilon_P = \text{constant}. \tag{54}$$

Here $\Pi_P(k) \sim k u_k \rho_k^2 = \text{const}$. As $u_k \sim k^{-1}$, this yields $\rho_k \sim \text{const}$. Hence, we argue that $E_P(k) \sim \rho_k^2/k \sim k^{-1}$. At these smaller scales, it is important to note that the degree of nonlinearity is expected to be higher for moderate stratification, which leads to $E_P(k) \sim k^{-1}$ and $\Pi_P(k) \sim \text{const}$, in contrast to $E_P(k) \sim k^{-3}$ and $\Pi_P(k) \sim k^{-2}$ for strongly stratified flows.

The KE and PE spectra as well as their fluxes are shown in Fig. 7. The KE spectrum $E_K(k)$ exhibits BO scaling, in particular, $E_K(k) \sim k^{-11/5}$ for $5 \le k \le 90$, and $E_K(k) \sim k^{-3}$ for $90 \le k \le 400$. The KE flux, seen in Fig. 7(b), also varies with scale; at large scales we see an inverse transfer (that scales approximately as $k^{-0.98}$) for $8 \le k \le 200$, while at small scales we obtain a forward transfer of KE for $200 \le k \le 1000$. The enstrophy flux is positive except for a narrow band near $k \approx 10$. Note that the PE spectrum [Fig. 7(a)] does not show dual scaling and scales approximately as $k^{-1.64}$; its flux is also not a constant but follows $\Pi_P(k) \sim k^{-0.3}$. We note that the behaviour of KE flux doesn't change at the same wavenumber as that of kinetic energy spectrum. At present, we believe that a higher resolution simulation is required to resolve the dual scaling issues.

At large scales, these scaling laws can be explained by replacing ϵ_P of Eqs. (42-44) with $\Pi_P(k) \sim k^{-0.3}$. This is similar to the variable flux arguments presented by Verma [46] and Verma and Reddy [61]. Specifically,

$$E_K(k) \sim k^{-0.3\times 2/5} k^{-11/5} \sim k^{-2.32}, \tag{55}$$
$$E_P(k) \sim k^{-0.3\times 4/5} k^{-7/5} \sim k^{-1.64}, \tag{56}$$
$$\Pi_K(k) \sim k^{-0.3\times 3/5} k^{-4/5} \sim k^{-0.98}. \tag{57}$$

Indeed, the spectral indices obtained above match those in Fig. 7 very closely.

At small scales the KE spectrum $E_K(k) \approx 2.0 \Pi_\omega^{2/3} k^{-3}$ that is associated with weaker buoyancy and constant enstrophy flux [see Fig. 7(a,b)], and are in accord with Eq. (51). Note that the spectra of the horizontal and vertical components of the flow also show dual scaling (see Fig. 8), thus suggesting the presence of an approximately isotropic flow at moderate stratification. As mentioned, the PE spectrum does not exhibit dual scaling, and we do not see

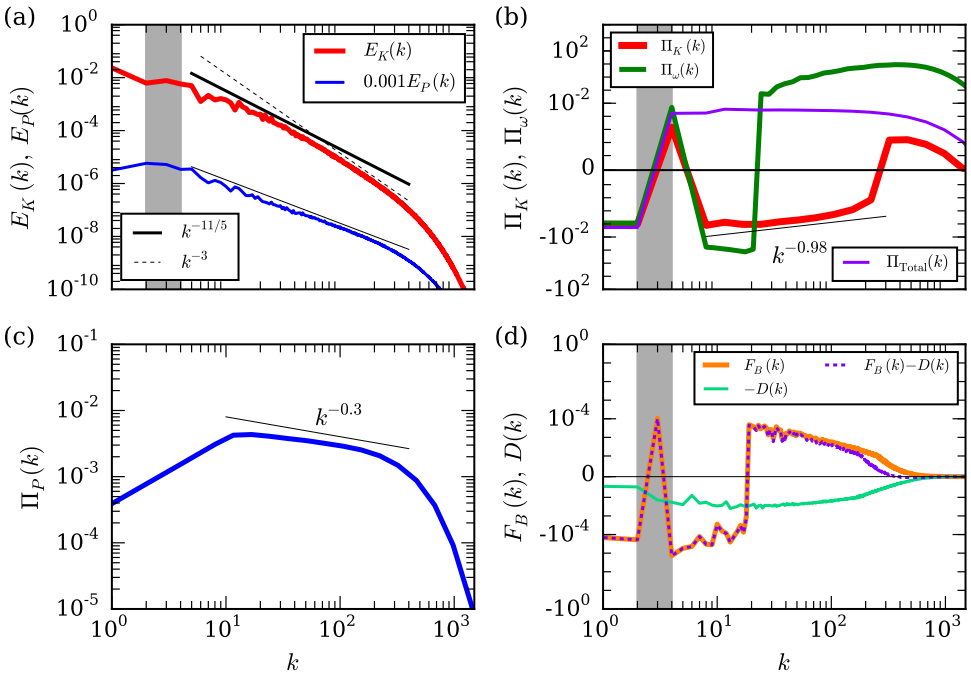

Figure 7: Moderate stratification (Fr = 0.37): (a) The KE and PE spectra. KE spectrum shows dual scaling with $k^{-11/5}$ and k^{-3}. The best fit for PE spectrum is $k^{-1.64}$ (thin black line); (b) KE flux $\Pi_K(k)$, enstrophy flux $\Pi_\omega(k)$, and total energy flux $\Pi_{\rm Total}(k)$; (c) PE flux; (d) $F_B(k)$, $D(k)$, and $F_B(k) - D(k)$.

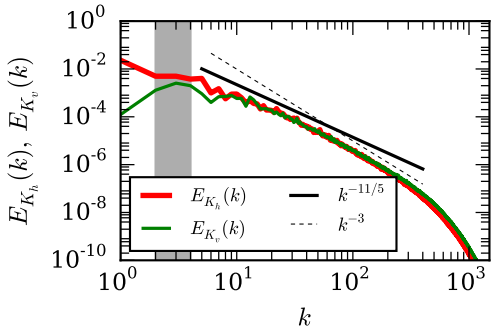

Figure 8: Plots for horizontal and vertical kinetic energy spectra for moderate stratification (Fr = 0.37). Both the spectra shows dual scaling similar to $E_K(k)$.

the k^{-1} scaling expected from Eq. (52) at small scales. Though, it should be noted that the PE flux is not constant but scales approximately as $k^{-0.3}$, and this implies a slightly steeper ($k^{-4/3}$) small scale PE spectrum. Indeed, a small change in scaling of this kind, i.e., -1.64 and -1.33 at large and small scales, respectively, may only be observable at a higher resolution.

The KE flux in the present 2D setting exhibits an inverse cascade, in contrast to the forward cascade in 3D [34]. Still the $k^{-11/5}$ spectrum of BO scaling is valid in 2D stably stratified turbulence due to the following reason. The energy supply due to buoyancy $F_B(k)$ and the dissipation rate $D(k)$, shown in Fig. 7(d), exhibit $F_B(k) > 0$ for $k > 20$, in contrast to 3D stably stratified flows for which $F_B(k) < 0$ [38]. From Eq. (31) we deduce that $|\Pi_K(k + \Delta k)| < |\Pi_K(k)|$ when $\Pi_K(k) < 0$ and $F_B(k) > 0$. Thus $|\Pi_K(k)|$ decreases with k and this yields Bolgiano scaling for the 2D moderately stratified flows. Physically, in Fig. 9 we observe ascending lighter fluid for which u_z and ρ are positively correlated. This is in contrast to 3D stably stratified flows for which $F_B(k) < 0$ due to a conversion of KE to PE [38]; i.e., there u_z and ρ are anti-correlated. Finally, it should be noted that even though KE flows upscale in this 2D setting, the total energy is transferred from large to small scales as seen by the total energy flux $\Pi_{\text{Total}}(k)$ in Fig. 7(b).

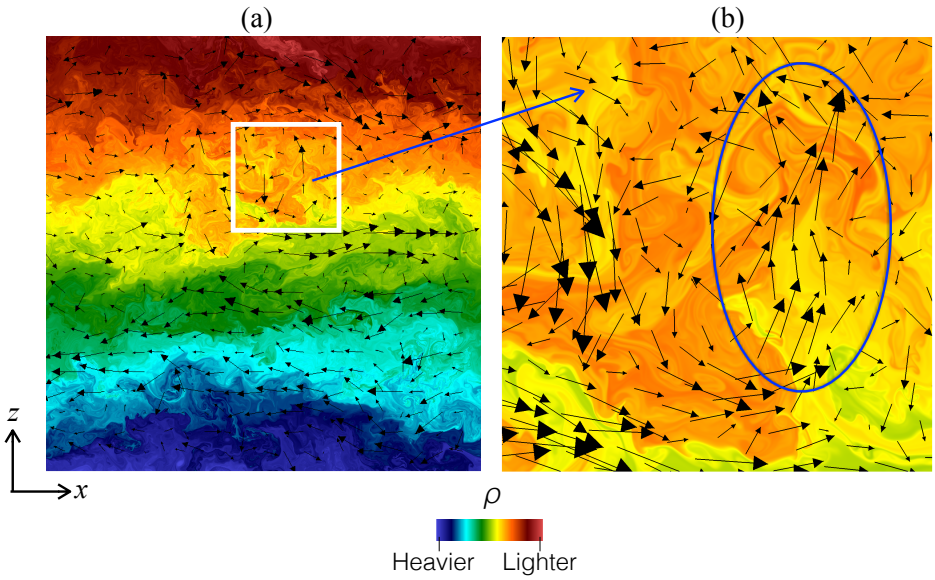

Figure 9: For Fr = 0.37 (a) the density plot of the density field ρ with the velocity field superimposed on it. In the boxed zone, lighter (higher) fluid ascends thus $F_B(k) \propto u_z\rho > 0$; (b) a zoomed view of the boxed zone.

4.3 Weak Stratification

Lastly we discuss the flow behaviour for weak stratification. In our simulations this is achieved for $\mathrm{Ra} = 10^8$, $\varepsilon = 0.3$ that yields $\mathrm{Fr} = 1.1$ and $\mathrm{Re} = 1.1 \times 10^4$. The flow pattern in Fig. 2 for $\mathrm{Fr} = 1.1$ shows a complete lack of a VSHF, instead, there is a tendency to form isotropic coherent structures similar to 2D hydrodynamic turbulence [50].

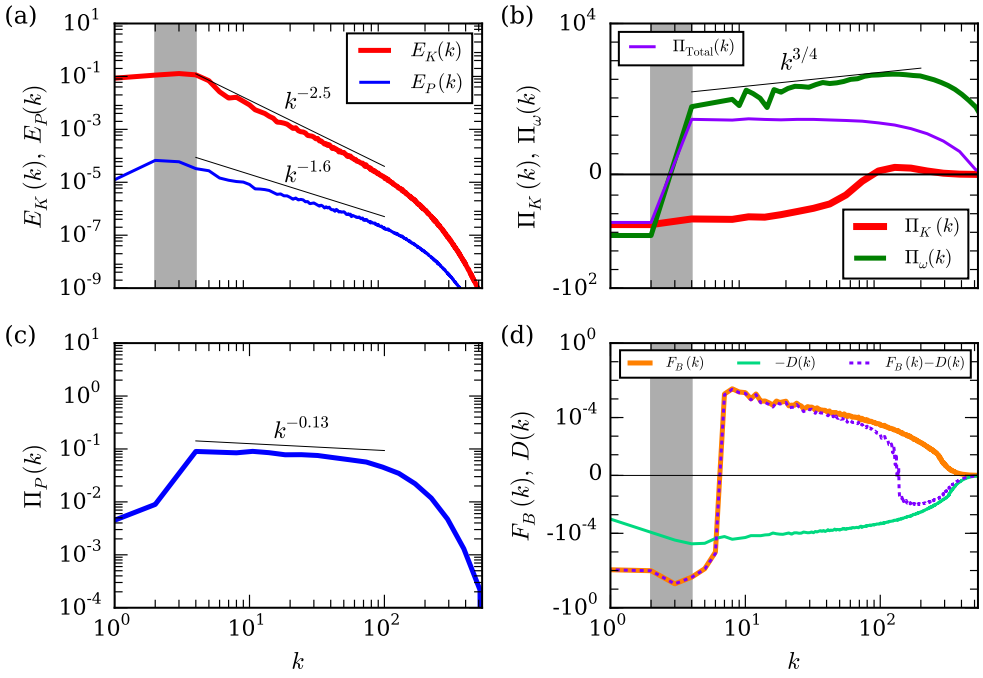

Figure 10: Weak stratification ($\mathrm{Fr} = 1.1$): (a) Plots of KE and PE spectra. KE spectrum $E_K(k)$ shows $k^{-2.5}$ scaling, while PE spectrum $E_P(k)$ shows $k^{-1.6}$ scaling; (b) Plots of KE flux $\Pi_K(k)$, enstrophy flux $\Pi_\omega(k)$, and total energy flux $\Pi_{\mathrm{Total}}(k)$; (c) PE flux $\Pi_P(k)$; (d) $F_B(k)$, $D(k)$, and $F_B(k) - D(k)$.

The energy spectra and fluxes for this case are shown in Fig. 10. Qualitatively similar to the moderate stratification case, we observe a negative KE flux at large scales. The enstrophy flux is strong and always positive, in fact it increases with wavenumber and scales approximately as $k^{3/4}$ up to the dissipation scale. This feature of the enstrophy flux alters the energy spectrum as follows,

$$E_K(k) \approx {\Pi_\omega}^{2/3} k^3 \sim k^{3/4\times 2/3-3} \sim k^{-2.5}, \tag{58}$$

which is in good agreement with our numerical finding, as shown in Fig. 10(a). Figure 11 presents the spectra of the horizontal and vertical components of

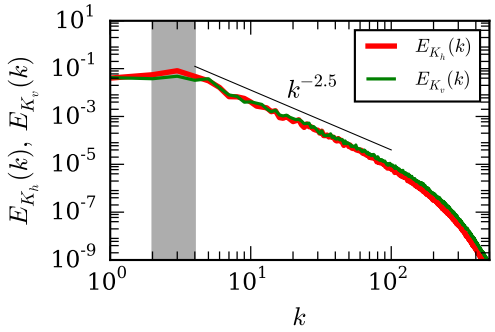

Figure 11: Plots for horizontal and vertical kinetic energy spectra for weak stratification (Fr = 1.1). Both the spectra, $E_{K_h}(k)$ and $E_{K_v}(k)$, overlap on each other similar to that of moderate stratification.

the flow, both are almost identical and scale as $E_{K_h}(k)$, $E_{K_v}(k) \sim k^{-2.5}$, thus confirming isotropy at all scales for weak stratification.

The PE spectrum $E_P(k) \sim k^{-1.6}$ and its flux Π_P is approximately constant with $\Pi_P(k) \sim k^{-0.13}$. Using $E_K(k) \sim k^{-2.5}$ and $\Pi_P(k) \approx k u_k \rho_k^2 \sim k^{-0.13}$, we obtain $E_P(k) \approx {\rho_k}^2/k \sim k^{-1.38}$, which is a little shallower than the $k^{-1.6}$ spectrum obtained in our numerical simulation. Once again, the total energy in the system flows from large to small scales [see Fig. 10(b)]. Taken together, the behaviour of KE and PE suggest that BO scaling may still be applicable for Fr = 1.1, though with a very restricted shallow $(-11/5)$ large-scale KE spectrum. Indeed, it would require much higher resolution to probe this issue. Finally, we remark that, to some extent, the forward (inverse) transfer of PE (KE) is reminiscent the flux loop scenario proposed by Boffetta *et al.* [27] for weakly stratified flows.

5 Summary and conclusions

We performed direct numerical simulations of 2D stably stratified flows under large-scale random forcing and studied the spectra and fluxes of kinetic energy, enstrophy, and potential energy. This is possibly the simplest non-trivial setting to explore the effects of stratification on fluid turbulence, much like surface turbulence in 3D flows which allow for an examination of compressibility on energy fluxes and spectra [62]. We find that the flows exhibit remarkably different behaviour as the strength of stratification is varied, and this is summarized in Table 3.

For strong stratification, as with numerous previous studies, we observe the emergence of a large-scale VSHF. This VSHF is explicitly identified as being composed of internal gravity waves, and further is seen to co-exist with smaller

Table 3: Scaling of KE spectrum $E_K(k)$, PE spectrum $E_P(k)$, KE flux $\Pi_K(k)$, PE flux $\Pi_P(k)$, and enstrophy flux $\Pi_\omega(k)$ for diffrent strength of stratification.

Strength of stratification	Spectrum	Flux
Strong	Large scale VSHF Small scale turbulence: $E_K(k) \sim k^{-3}$ $E_P(k) \sim k^{-3}$	 $\Pi_K(k) \sim 0$ $\Pi_\omega(k) \sim$ const. $\Pi_P(k) \sim k^{-2}$
Moderate	For $5 \leq k \leq 90$: $E_K(k) \sim k^{-2.2}$ $E_P(k) \sim k^{-1.64}$ For $90 \leq k \leq 400$: $E_K(k) \sim k^{-3}$ $E_P(k) \sim k^{-1.64}$	 $\Pi_K(k) \sim k^{-0.98}$ (Negative) $\Pi_\omega(k) \sim$ const. $\Pi_P(k) \sim k^{-0.3}$ $\Pi_K(k)$: weak (positive) $\Pi_\omega(k) \sim$ const. $\Pi_P(k) \sim k^{-0.3}$
Weak	$E_K(k) \sim k^{-2.5}$ $E_P(k) \sim k^{-1.6}$	$\Pi_K(k) \sim$ const. (Negative) $\Pi_\omega(k) \sim k^{3/4}$ $\Pi_P(k) \sim k^{-0.13}$

scale turbulence. The turbulent portion of the flow follows some aspects of the traditional enstrophy cascading regime of pure 2D turbulence. In particular, we find a strong, nearly constant, positive enstrophy flux, zero KE flux and KE spectrum that scales approximately as k^{-3}. But, the PE does not act as a passive scalar. Indeed, it exhibits an approximate k^{-3} spectrum and a scale dependent k^{-2} forward flux. In addition, the flow in the strongly stratified regime is highly anisotropic and the horizontal and vertical flow spectra follow $E_{K_h}(k) \sim k^{-3}$ and $E_{K_v}(k) \sim k^{-5}$ scaling, respectively.

Moderate stratification proves to be very interesting, specifically, there is no VSHF and we observe a modified BO scaling for the KE — $E_K(k) \sim k^{-11/5}$ at large scales and an approximate k^{-3} power-law at small scales. Further, the nature of the KE flux also changes, with the upscale or inverse transfer at large scales and a weak forward transfer at smaller scales. The PE, on the other hand, always flows downscale and its flux is weakly scale dependent (approximately $k^{-0.3}$). The PE spectrum scales as $k^{-1.64}$, with no signs of a dual scaling like the KE. But, as the expected change in scaling of the PE spectrum is small, it is possible that higher resolution simulations may prove to be useful in this regard.

Weak stratification also differs significantly from pure 2D turbulence. In particular, we actually see a positive scale dependent enstrophy flux ($\sim k^{3/4}$) up to the dissipation scale. In agreement with this form of the enstrophy flux, the KE spectrum scales approximately as $k^{-2.5}$. The KE flux is robustly negative, and the inverse transfer begins at a comparatively smaller scale than with moderate stratification. The PE flux, once again, is positive and almost scale independent, and the PE spectrum follows an approximate $k^{-1.6}$ scaling law.

Thus, the nature of 2D stably stratified turbulence under large scale random forcing is dependent on the strength of the ambient stratification. Despite this diversity, we do observe some universal features. Specifically, the total and potential energy always flow downscale, which is in agreement with 3D stratified turbulence. The KE almost never shows a forward transfer (apart from the weak downscale transfer at small scales in moderate stratification). In addition, the zero flux of KE in strong stratification, and its upscale transfer at large scales in moderate and weakly stratified cases is in contrast to the 3D scenario. Finally, apart from the PE spectrum for weak stratification (and its small scale behaviour for moderate stratification), the scaling exponents observed very closely match dimensional expectations when we take into account the scale dependent form of the corresponding flux.

Acknowledgements

We thank Anirban Guha for useful discussions. Our numerical simulations were performed on *Chaos* clusters of IIT Kanpur and "Shaheen II" at KAUST supercomputing laboratory, Saudi Arabia. This work was supported by a research grant (Grant No. SERB/F/3279) from Science and Engineering Research Board, India, computational project k1052 from KAUST, and the grant

PLANEX/PHY/2015239 from Indian Space Research Organisation (ISRO), India. JS would also like to acknowledge support from the IISc ISRO Space Technology Cell project ISTC0352 and the Ministry of Earth Sciences Monsoon Mission grant IITM/MAS/DSG/0001.

References

[1] G.K. Vallis *Atmospheric and Oceanic Fluid Dynamics*, Cambridge University Press, Cambridge, 2006.

[2] J. Riley, and M. LeLong, *Fluid motions in the presence of strong stable stratification*, Ann. Rev. Fluid Mech. 32 (2000), pp. 613–657.

[3] D. Lilly, *Stratified turbulence and the mesoscale variability of the atmosphere*, J. Atmos. Sci. 40 (1983), pp. 749–761.

[4] E.J. Hopfinger, *Turbulence in stratified fluids: A review*, J. Geophys. Res. 92 (1987), pp. 5287–5303.

[5] C. Leith, *Normal mode initialization and quasigeostrophic theory*, J. Atmos. Sci. 37 (1980), pp. 958–968.

[6] P. Embid, and A. Majda, *Low Froude number limiting dynamics for stably stratified flow with small or finite Rossby numbers*, Geophys. Astrophys. Fluid Dynamics 87 (1998), pp. 1–50.

[7] M. LeLong, and J. Riley, *Internal wave-vortical mode interactions in strongly stratified flows*, J. Fluid Mech. 232 (1991), pp. 1–19.

[8] J.P. Laval, J. McWilliams, and B. Dubrulle, *Forced stratified turbulence: Successive transitions with Reynolds number*, Phys. Rev. E 68 (2003), p. 036308.

[9] M.L. Waite, and P. Bartello, *Stratified turbulence dominated by vortical motion*, J. Fluid Mech. 517 (2004), p. 281.

[10] M.L. Waite, and P. Bartello, *Stratified turbulence generated by internal gravity waves*, J. Fluid Mech. 546 (2006), p. 313.

[11] E. Lindborg, and G. Brethouwer, *Stratified turbulence forced in rotational and divergent modes*, J. Fluid Mech. 586 (2007), pp. 83–108.

[12] P. Bartello, *Geostrophic adjustment and inverse cascades in rotating stratified turbulence*, J. Atmos. Sci. 52 (1995), pp. 4410–4428.

[13] L. Smith, and F. Waleffe, *Generation of slow large scales in forced rotating stratified turbulence*, J. Fluid. Mech. 451 (2002), pp. 145–168.

[14] Y. Kitamura, and Y. Matsuda, *The k_h^{-3} and $k_h^{-5/3}$ energy spectra in stratified turbulence*, Geophys. Res. Lett. 33 (2006), p. L05809.

[15] J. Sukhatme, and L. Smith, *Vortical and wave modes in 3D rotating stratified flows: Random large-scale forcing*, Geophys. Astrophys. Fluid Dynamics 102 (2008), pp. 437–455.

[16] A. Vallgren, E. Deusebio, and E. Lindborg, *Possible explanation of the atmospheric kinetic and potential energy spectra*, Phys. Rev. Lett. 107 (2011), p. 268501.

[17] R. Marino, D. Rosenberg, C. Herbert, and A. Pouquet, *Interplay of waves and eddies in rotating stratified turbulence and the link with kinetic-potential energy partition*, EPL 112 (2015), p. 49001.

[18] G. Carnevale, and J. Frederiksen, *A statistical dynamical theory of strongly nonlinear internal gravity waves*, Geophys. Astrophys. Fluid Dynamics 23 (1983), pp. 175–207.

[19] J. Frederiksen, and R. Bell, *Statistical dynamics of internal gravity waves - turbulence*, Geophys. Astrophys. Fluid Dynamics 26 (1983), pp. 257–301.

[20] Y. Lvov, and N. Yokoyama, *Nonlinear wave-wave interactions in stratified flows: Direct numerical simulations*, Physica D 238 (2009), pp. 803–815.

[21] M. Remmel, J. Sukhatme, and L. Smith, *Nonlinear gravity wave interactions in stratified turbulence*, Theor. Comput. Fluid Dyn. (2013).

[22] D. Benielli, and J. Sommeria, *Excitation of internal waves and stratified turbulence by parametric instability*, Dyn. Atmos. Oceans 23 (1996), pp. 335–343.

[23] P. Bouruet-Aubertot, J. Sommeria, and C. Staquet, *Breaking of standing internal gravity waves through two-dimensional instabilities* , J. Fluid Mech. 285 (1995), pp. 265–301.

[24] P. Bouruet-Aubertot, J. Sommeria, and C. Staquet, *Stratified turbulence produced by internal wave breaking: Two-dimensional numerical experiments*, Dyn. Atmos. Oceans 23 (1996), pp. 357–369.

[25] J. Sukhatme, and L.M. Smith, *Self-similarity in decaying two-dimensional stably stratified adjustment*, Phys. Fluids 19 (2007), p. 036603.

[26] L.M. Smith, *Numerical study of two-dimensional stratified turbulence*, Contemp. Math. 283 (2001), p. 91.

[27] G. Boffetta, F. de Lillo, A. Mazzino, and S. Musacchio, *A flux loop mechanism in two-dimensional stratified turbulence*, EPL 95 (2011), p. 34001.

[28] J. Sukhatme, A.J. Majda, and L.M. Smith, *Two-dimensional moist stratified turbulence and the emergence of vertically sheared horizontal flows*, Phys. Fluids 24 (2012), pp. 036602–16.

[29] J. Zhang, X.L. Wu, and K.Q. Xia, *Density fluctuations in strongly stratified two-dimensional turbulence*, Phys. Rev. Lett. 94 (2005), p. 174503.

[30] R. Bolgiano, *Turbulent spectra in a stably stratified atmosphere*, J. Geophys. Res. 64 (1959), p. 2226.

[31] A.N. Obukhov, *Effect of Archimedean forces on the structure of the temperature field in a turbulent flows*, Dokl. Akad. Nauk SSSR 125 (1959), p. 1246.

[32] G.K. Batchelor, *Small scale variation of convected quantities like temperature in a turbulent fluid*, J. Fluid Mech. 5 (1959), p. 113.

[33] F. Seychelles, Y. Amarouchene, M. Bessafi, and H. Kellay, *Thermal convection and emergence of isolated vortices in soap bubbles*, Phys. Rev. Lett. 100 (2008), pp. 144501–4.

[34] E. Lindborg, *The energy cascade in a strongly stratified fluid*, J. Fluid Mech. 550 (2006), p. 207.

[35] G. Brethouwer, P. Billant, E. Lindborg, and J.M. Chomaz, *Scaling analysis and simulation of strongly stratified turbulent flows*, J. Fluid Mech. 585 (2007), p. 343.

[36] P. Bartello, and S.M. Tobias, *Sensitivity of stratified turbulence to the buoyancy Reynolds number*, J. Fluid Mech. 725 (2013), pp. 1–22.

[37] M.K. Verma, A.G. Chatterjee, K.S. Reddy, R.K. Yadav, S. Paul, M. Chandra, and R. Samtaney, *Benchmarking and scaling studies of a pseudospectral code Tarang for turbulence simulations*, Pramana 81 (2013), pp. 617–629.

[38] A. Kumar, A.G. Chatterjee, and M.K. Verma, *Energy spectrum of buoyancy-driven turbulence*, Phys. Rev. E 90 (2014), p. 023016.

[39] B. Sutherland *Internal Gravity Waves*, Cambridge University Press, Cambridge, 2010.

[40] E. Lindborg, and G. Brethouwer, *Vertical dispersion by stratified turbulence*, J. Fluid Mech. 614 (2008), pp. 303–314.

[41] R. Kraichnan, *Inertial ranges in two-dimensional turbulence*, Phys. Fluids 10 (1967), p. 1417.

[42] M.E. Maltrud, and G.K. Vallis, *Energy spectra and coherent structures in forced two-dimensional and beta-plane turbulence*, J. Fluid Mech. 228 (1991), p. 321.

[43] L. Smith, and V. Yakhot, *Bose condensation and small-scale structure generation in a random force driven 2D turbulence.*, Phys. Rev. Lett. 71 (1993), pp. 352–355.

[44] V. Borue, *Spectral exponents of enstrophy cascade in stationary two-dimensional homogeneous turbulence*, Phys. Rev. Lett. 71 (1993), pp. 3967–3970.

[45] E. Lindborg, and K. Alvelius, *The kinetic energy spectrum of the two-dimensional enstrophy turbulence cascade*, Phys. Fluids 12 (2000), pp. 945–4.

[46] M.K. Verma, *Variable enstrophy flux and energy spectrum in two-dimensional turbulence with Ekman friction*, EPL 98 (2012), p. 14003.

[47] M. Lesieur *Turbulence in Fluids - Stochastic and Numerical Modelling*, Kluwer Academic Publishers, Dordrecht, 2008.

[48] G. Dar, M. Verma, and V. Eswaran, *Energy transfer in two-dimensional magnetohydrodynamic turbulence: Formalism and numerical results*, Physica D 157 (2001), pp. 207–225.

[49] M.K. Verma, *Statistical theory of magnetohydrodynamic turbulence: Recent results*, Phys. Rep. 401 (2004), pp. 229–380.

[50] J. McWilliams, *The emergence of isolated coherent vortices in turbulent flow*, J. Fluid Mech. 146 (1984), pp. 21–43.

[51] P. Billant, and J.M. Chomaz, *Self-similarity of strongly stratified inviscid flows*, Phys. Fluids 13 (2001), p. 1645.

[52] G. Boffetta, *Energy and enstrophy fluxes in the double cascade of two-dimensional turbulence*, J. Fluid Mech. 589 (2007), p. 8.

[53] G. Boffetta, and S. Musacchio, *Evidence for the double cascade scenario in two-dimensional turbulence*, Phys. Rev. E 82 (2010), p. 016307.

[54] G. Boffetta, and R.E. Ecke, *Two-dimensional turbulence*, Annu. Rev. Fluid Mech. 44 (2012), pp. 427–451.

[55] M.C. Jullien, P. Castiglione, and P. Tabeling, *Experimental observation of Batchelor dispersion of passive tracers*, Phys. Rev. Lett. 85 (2000), pp. 3636–3639.

[56] F. Zonta, M. Onorato, and A. Soldati, *Turbulence and internal waves in stably-stratified channel flow with temperature-dependent fluid properties*, J. Fluid Mech. 697 (2012), pp. 175–203.

[57] A. Kumar, and M.K. Verma, *Shell model for buoyancy-driven turbulence*, Phys. Rev. E 91 (2015), p. 043014.

[58] M.K. Verma, A. Kumar, and A.G. Chatterjee, *Energy spectrum and flux of buoyancy-driven turbulence*, Physics Focus, AAPPS Bulletin 25 (2015).

[59] J.K. Bhattacharjee, *Kolmogorov argument for the scaling of the energy spectrum in a stratified fluid*, Phys. Lett. A 379 (2015), pp. 696–699.

[60] D. Rosenberg, A. Pouquet, R. Marino, and P.D. Mininni, *Evidence for Bolgiano-Obukhov scaling in rotating stratified turbulence using high-resolution direct numerical simulations*, Phys. Fluids 27 (2015), pp. 055105–25.

[61] M.K. Verma, and K.S. Reddy, *Modeling quasi-static magnetohydrodynamic turbulence with variable energy flux*, Phys. Fluids (2015), p. 025114.

[62] S. Lovecchio, F. Zonta, and A. Soldati, *Upscale energy transfer and flow topology in free-surface turbulence*, Phys. Rev. E 91 (2015), p. 033010.